

Thermalisation of light sterile neutrinos in the early universe

Steen Hannestad,^a Irene Tamborra^b and Thomas Tram^a

^aDepartment of Physics and Astronomy, University of Aarhus, 8000 Aarhus C, Denmark

^bMax-Planck-Institut für Physik (Werner-Heisenberg-Institut)
Föhringer Ring 6, 80805 München, Germany

E-mail: sth@phys.au.dk, tamborra@mpp.mpg.de, tram@phys.au.dk

Abstract. Recent cosmological data favour additional relativistic degrees of freedom beyond the three active neutrinos and photons, often referred to as “dark” radiation. Light sterile neutrinos is one of the prime candidates for such additional radiation. However, constraints on sterile neutrinos based on the current cosmological data have been derived using simplified assumptions about thermalisation of ν_s at the Big Bang Nucleosynthesis (BBN) epoch. These assumptions are not necessarily justified and here we solve the full quantum kinetic equations in the (1 active + 1 sterile) scenario and derive the number of thermalised species just before BBN begins ($T \simeq 1$ MeV) for null ($L = 0$) and large ($L = 10^{-2}$) initial lepton asymmetry and for a range of possible mass-mixing parameters. We find that the full thermalisation assumption during the BBN epoch is justified for initial small lepton asymmetry only. Partial or null thermalisation occurs when the initial lepton asymmetry is large.

Contents

1	Introduction	1
2	Equations of motion	2
2.1	Quantum Kinetic Equations	2
2.2	Mapping with the active and the sterile variables	4
3	Results: thermalised sterile species	6
3.1	Numerical solution of the quantum kinetic equations	6
3.2	Sterile neutrino production for zero lepton asymmetry	7
3.3	The case of large initial lepton asymmetry	10
4	Conclusions	12
A	Location of the resonances	14
B	Adiabatic approximation	15

1 Introduction

Sterile neutrinos are hypothetical $SU(2) \times U(1)$ singlets. They are supposed to mix with one or more of the active states without interacting with any other particle. Low-mass sterile neutrinos have been invoked to explain the excess $\bar{\nu}_e$ events in the LSND experiment [1–3] as well as the MiniBooNE excess events in both neutrino and antineutrino channels. Interpreted in terms of flavour oscillations, the MiniBooNE data require CP violation and thus no less than two sterile families [4–6] or additional ingredients such as non-standard interactions [7]. Recently a new analysis of reactor $\bar{\nu}_e$ spectra and their distance and energy variation [8–10] suggested indication for the possible existence of eV-mass sterile neutrinos. However the IceCube collaboration excluded part of the parameter space [11].

The most recent analysis of cosmological data suggest a trend towards the existence of “dark radiation,” radiation in excess with respect to the three neutrino families and photons [12–14]. The cosmic radiation content is usually expressed in terms of the effective number of thermally excited neutrino species, N_{eff} . Its standard value, $N_{\text{eff}} = 3.046$, slightly exceeds 3 because of e^+e^- annihilation providing residual neutrino heating [15]. The Wilkinson Microwave Anisotropy Probe (WMAP) collaboration found $N_{\text{eff}} = 4.34^{+0.86}_{-0.88}$ based on their 7-year data release and additional LSS data [16] at 1σ . Including the Sloan Digital Sky Survey (SDSS) data release 7 (DR7) halo power spectrum, [13] found $N_{\text{eff}} = 4.78^{+1.86}_{-1.79}$ at 2σ . Measurements of the CMB anisotropy on smaller scales by the ACT [17] and SPT [18] collaborations also find tentative evidence for a value of N_{eff} higher than predicted by the standard model (see also [19–23] for recent discussions of N_{eff}).

Also, cosmological constraints coming from big bang nucleosynthesis (BBN) suggest that the relatively high ^4He abundance can be interpreted in terms of additional radiation during the BBN epoch [24, 25]. Low-mass sterile neutrinos have been considered among possible candidates for the extra-radiation content [26–28]. The cosmic microwave background

anisotropies and big-bang nucleosynthesis in combination seem to favor an excess of radiation compatible with one family of sub-eV sterile neutrinos [14, 27–29]. On the other hand, eV-mass sterile neutrinos are cosmologically viable only if additional ingredients are included since otherwise sterile neutrinos would contribute too much hot dark matter [26] (see also [30]).

However, cosmological constraints during the BBN epoch have usually been derived under the assumption that the extra sterile neutrino families were fully thermalised [26]. However, the validity of this assumption is not a priori clear and some preliminary studies [31, 32] already pointed toward this direction. It was shown in [33] that for plausible values of the mass and mixing parameters, and initial lepton asymmetries not excluded by current observations there are cases where little or no thermalisation occurs. For the charged fermions of the standard model the particle anti-particle asymmetry is known to be of order 10^{-10} . For neutrinos, however, no such bound exists, and the asymmetry can be many orders of magnitude larger without violating observational constraints. In the standard model with no sterile states the upper bound on the neutrino chemical potential is of order $\mu/T \lesssim \text{few} \times 10^{-2}$ [34–39] and while no exact bound has been derived in models with sterile neutrinos, we expect that the upper bound is of the same order of magnitude.

The purpose of this paper is to quantitatively derive the amount of thermalisation as a function of neutrino parameters (mass, mixing, and initial lepton asymmetry). We solve the full quantum kinetic equations in the 1 active+1 sterile approximation, calculate the effective number of thermalised species just before BBN starts (at $T \simeq 1$ MeV) and define under which conditions the thermalisation hypothesis holds. The assumption of (1+1) families to evaluate the thermalisation degree is justified for small lepton asymmetries since the resonances in the active sector are decoupled from the conversions occurring in the active-sterile sector due to the larger mass difference. However, for large asymmetries active-sterile conversion is delayed and can occur simultaneously with active-active conversion. While this does not qualitatively change the overall picture there are some issues which we will return to in Section 3.

In our study, we calculate the number of thermalised extra families for the allowed mass-mixing parameter space for different initial lepton asymmetries. In Section 2 we introduce the adopted formalism and the quantum kinetic equations. In Section 3, we present our results for initial null and large ($L = 10^{-2}$) lepton asymmetry. Conclusions and perspectives are presented in Section 4.

2 Equations of motion

In this section, we introduce the quantum kinetic equations (QKEs) governing the evolution of neutrinos in the early universe [40–45]. We adopt a mapping of the Bloch vectors in terms of new vectors related to the active and sterile species grouping large and small dynamical variables.

2.1 Quantum Kinetic Equations

We consider oscillations of one active flavour ν_a (with $a = e$ or μ, τ) with a sterile neutrino state ν_s . Denoting with θ_s the mixing angle in vacuum and with ν_1 and ν_2 the two mass eigenstates, separated by the mass difference δm_s^2 , we have:

$$\nu_a = \cos \theta_s \nu_1 - \sin \theta_s \nu_2 , \quad (2.1)$$

$$\nu_s = \sin \theta_s \nu_1 + \cos \theta_s \nu_2 . \quad (2.2)$$

In what follows we will refer $\delta m_s^2 > 0$ as the normal hierarchy scenario (NH) and $\delta m_s^2 < 0$ as the inverted hierarchy scenario (IH). Structure formation data strongly disfavour models with a total thermalised neutrino mass (the sum of all fully thermalised mass states) in excess of 0.5-1 eV. Given that all the active states are fully thermalised this disfavors the inverted hierarchy for sterile masses above 0.2-0.3 eV. However, for masses below this the inverted hierarchy is not disfavoured and for completeness we study the same mass and mixing parameter space for both NH and IH.

In order to describe the evolution of sterile neutrinos in the early universe, we use the density matrix formalism and we express the density matrix associated with each momentum p in terms of the Bloch vector components $(P_0, \mathbf{P}) = (P_0, P_x, P_y, P_z)$ [40, 41, 43],

$$\rho = \frac{1}{2} f_0 (P_0 + \mathbf{P} \cdot \sigma), \quad \bar{\rho} = \frac{1}{2} f_0 (\bar{P}_0 + \bar{\mathbf{P}} \cdot \sigma), \quad (2.3)$$

where σ are the Pauli matrices and $f_0 = 1/(1 + e^{p/T})$ is the Fermi-Dirac distribution function with no chemical potential. The neutrino kinetic equations in terms of the components of the Bloch vectors for each momentum mode are:

$$\dot{\mathbf{P}} = \mathbf{V} \times \mathbf{P} - D(P_x \mathbf{x} + P_y \mathbf{y}) + \dot{P}_0 \mathbf{z}, \quad (2.4)$$

$$\dot{P}_0 = \Gamma \left[\frac{f_{\text{eq}}}{f_0} - \frac{1}{2}(P_0 + P_z) \right] \quad (2.5)$$

where the dot denotes the time derivative ($d_t = \partial_t - Hp\partial_p$, with H the Hubble parameter) and $f_{\text{eq}} = 1/(1 + e^{(p-\mu)/T})$.

Defining the comoving momentum $x = p/T$, the vector \mathbf{V} has the following components

$$V_x = \frac{\delta m_s^2}{2xT} \sin 2\theta_s, \quad (2.6)$$

$$V_y = 0, \quad (2.7)$$

$$V_z = V_0 + V_1 + V_L. \quad (2.8)$$

and

$$V_0 = -\frac{\delta m_s^2}{2xT} \cos 2\theta_s, \quad (2.9)$$

$$V_1^{(a)} = -\frac{7\pi^2}{45\sqrt{2}} \frac{G_F}{M_Z^2} x T^5 [n_{\nu_a} + n_{\bar{\nu}_a}] g_a \quad (2.10)$$

$$V_L = \frac{2\sqrt{2}\zeta(3)}{\pi^2} G_F T^3 L^{(a)}. \quad (2.11)$$

Here, $g_{\mu,\tau} = 1$ for $\nu_{\mu,\tau} - \nu_s$ mixing, $g_e = 1 + 4 \sec^2 \theta_W / (n_{\nu_e} + n_{\bar{\nu}_e})$ for $\nu_e - \nu_s$ mixing and θ_W is the Weinberg angle. The dimensionless number densities $n_{\nu_a, (\bar{\nu}_a)}$ are the equilibrium active neutrino (antineutrino) densities normalised to unity in thermal equilibrium. The effective neutrino asymmetries $L^{(a)}$ are defined by

$$L^{(e)} = \left(\frac{1}{2} + 2 \sin^2 \theta_W \right) L_e + \left(\frac{1}{2} - 2 \sin^2 \theta_W \right) L_p - \frac{1}{2} L_n + 2L_{\nu_e} + L_{\nu_\mu} + L_{\nu_\tau}, \quad (2.12)$$

$$L^{(\mu)} = L^{(e)} - L_e - L_{\nu_e} + L_{\nu_\mu}, \quad (2.13)$$

$$L^{(\tau)} = L^{(e)} - L_e - L_{\nu_e} + L_{\nu_\tau}, \quad (2.14)$$

where $L_f \equiv (n_f - n_{\bar{f}})N_f/N_\gamma$ with N_f (N_γ) the integrated active (photon) number density in thermal equilibrium. The potential V_L , defined as in Eq. (2.11), is the leading order contribution to V_z . The V_1 term is the finite temperature correction and for example in the case of ν_e - ν_s mixing it includes coherent interactions of ν_e with the medium through which it propagates. The condition for a matter induced resonance to occur is $V_z = 0$, and because V_z depends on $L^{(a)}$ any non-zero lepton asymmetry can have dramatic consequences for oscillation driven active-sterile neutrino conversion. In Appendix A we discuss the location of resonances in detail for all possible values of mass, mixing, and lepton asymmetry.

A detailed derivation of the quantum kinetic equations is presented in [42, 46]. Here we choose to adopt minimal assumptions on the collision terms. In particular, the term D is the damping term, quantifying the loss of quantum coherence due to ν_a collisions with the background medium. For example, considering ν_e , the elastic contribution should come from the elastic scattering of ν_e with e^- and e^+ and with the other active flavours ν_a and $\bar{\nu}_a$. The inelastic contribution comes from the scattering of ν_e with $\bar{\nu}_e$ (producing e^- and e^+ or ν_a and $\bar{\nu}_a$). In terms of the Bloch vectors such terms have the effect of suppressing the off-diagonal elements of the density matrix ($P_{x,y}$). The effective potentials contributing to this term have been previously calculated [46–48] and if thermal equilibrium is assumed and the electron mass neglected, it is approximately half the corresponding scattering rate Γ [40, 42, 49]

$$D = \frac{1}{2}\Gamma . \quad (2.15)$$

The evolution of P_0 is determined by processes that deplete or enhance the abundance of ν_a with the same momentum and its rate of change receives no contribution from coherent ν_a - ν_s oscillations. The repopulation term $\Gamma(f_{\text{eq}}/f_0 - 1/2(P_0 + P_z))$ is an approximation for the correct elastic collision integral [49] with

$$\Gamma = C_a G_F^2 x T^5 \quad (2.16)$$

where $C_e \simeq 1.27$ and $C_{\mu,\tau} \simeq 0.92$ [41]. Note that the term including the effective collision rate, Γ , is an approximation to the full momentum dependent scattering kernel which repopulates neutrinos from the background plasma. The full expression has been derived in [42]. In [49] it was proven that the general form of D (and Γ) exactly reduces to Eqs. (2.15,2.16) for weakly interacting species in thermal equilibrium with zero chemical potential, and that it is the zero order approximation for particles with non-null chemical potential. The respective equations of motion for anti-neutrinos can be found by substituting $L^{(a)} = -L^{(a)}$ and $\mu = -\mu$ in the above equations. In our treatment we have not included the rate equations for the electrons and positrons since we are assuming that all the species electromagnetically interacting are kept in equilibrium.

2.2 Mapping with the active and the sterile variables

We can distinguish among large and small linear combinations of the dynamical variables in the particle and antiparticle sector to simplify the numerical treatment. For each momentum mode, we define for each component i (with $i = 0, x, y, z$) of the Bloch vector

$$P_i^\pm = P_i \pm \bar{P}_i . \quad (2.17)$$

We also separate active (a) and sterile (s) sectors

$$P_a^\pm = P_0^\pm + P_z^\pm = 2\frac{\rho_{aa}^\pm}{f_0}, \quad (2.18)$$

$$P_s^\pm = P_0^\pm - P_z^\pm = 2\frac{\rho_{ss}^\pm}{f_0}. \quad (2.19)$$

Therefore, in terms of the new vectors Eqs. (2.4, 2.5) become

$$\dot{P}_a^\pm = V_x P_y^\pm + \Gamma [2f_{eq}^\pm/f_0 - P_a^\pm], \quad (2.20)$$

$$\dot{P}_s^\pm = -V_x P_y^\pm, \quad (2.21)$$

$$\dot{P}_x^\pm = -(V_0 + V_1)P_y^\pm - V_L P_y^\mp - D P_x^\pm, \quad (2.22)$$

$$\dot{P}_y^\pm = (V_0 + V_1)P_x^\pm + V_L P_x^\mp - \frac{1}{2}V_x(P_a^\pm - P_s^\pm) - D P_y^\pm, \quad (2.23)$$

where we have defined $f_{eq}^\pm = f_{eq}(p, \mu) \pm f_{eq}(p, -\mu)$.

The lepton number can be directly calculated from the integral over the difference between the neutrino and the antineutrino distribution functions, i.e. P_a^- :

$$L^{(a)} = \frac{2}{8\zeta(3)} \int_0^\infty dx x^2 \rho_{aa}^- = \frac{1}{8\zeta(3)} \int_0^\infty dx x^2 f_0 P_a^-. \quad (2.24)$$

However, since the repopulation term is approximated by Eq. (2.16) which does not explicitly conserve lepton number we independently evolve $L^{(a)}$ as in [50] using an evolution equation where the repopulation term does not enter. Taking the time derivative of Eq. (2.24) and ignoring the repopulation part of \dot{P}_a^- , the evolution equation for $L^{(a)}$ is

$$\dot{L}^{(a)} = \frac{1}{8\zeta(3)} \int_0^\infty dx x^2 f_0 V_x P_y^-. \quad (2.25)$$

Note that, in kinetic equilibrium, μ , or rather the degeneracy parameter $\xi \equiv \mu/T$, is related to the lepton number $L^{(a)}$ through the integral over f_{eq}^- [34]

$$L_{eq}^{(a)} = \frac{1}{4\zeta(3)} \int_0^\infty dx x^2 \left[\frac{1}{1 + e^{x-\xi}} - \frac{1}{1 + e^{x+\xi}} \right] = \frac{1}{12\zeta(3)} (\pi^2 \xi + \xi^3). \quad (2.26)$$

This is a third order equation, and using Chebyshev's cubic root, one can extract the corresponding expression for ξ valid for any $L^{(a)}$ using trigonometric functions:

$$\xi = \frac{-2\pi}{\sqrt{3}} \sinh \left(\frac{1}{3} \operatorname{arcsinh} \left[-\frac{18\sqrt{3}\zeta(3)}{\pi^3} L^{(a)} \right] \right). \quad (2.27)$$

In order to numerically solve the QKEs, we define the momentum grid in comoving coordinates ($x = p/T$). Therefore the grid becomes stationary and the partial differential equations become ordinary differential equations coupled through integrated quantities only. Using the temperature T as the evolution parameter, time derivatives, d_t , are replaced by $\rightarrow -HT\partial_T$ in the above equations, provided that the time derivative of the effective number of degrees of freedom can be ignored.

3 Results: thermalised sterile species

The fraction of sterile thermalised species is defined as

$$\delta N_{\text{eff},s} = \frac{\int dx x^3 f_0 P_s^+}{4 \int dx x^3 f_0}. \quad (3.1)$$

However, the total amount of radiation is given by the sum of active and sterile energy densities

$$\delta N_{\text{eff}} = \frac{\int dx x^3 f_0 (P_s^+ + P_a^+ - 4)}{4 \int dx x^3 f_0}. \quad (3.2)$$

Note that when the active state is in thermal equilibrium ($P_a^+ = 4$), $\delta N_{\text{eff},s} = \delta N_{\text{eff}}$. When $L^{(a)}$ is large, the sterile sector may be populated so late that the active sector does not have time to repopulate before it decouples. In this section, we discuss the fraction of thermalised species for initial $L^{(a)} = 0$ and $L^{(a)} = 10^{-2}$ and for a range of $(\delta m_s^2, \sin^2 2\theta_s)$.

In terms of late-time cosmological constraints on light neutrinos both $\delta N_{\text{eff},s}$ and δN_{eff} can be relevant quantities. Models with a modified light neutrino sector are most often parametrised in terms of the neutrino mass, m_ν , and N_{eff} in such a way that N_{eff} neutrino species all share the same common mass m_ν (i.e. it is assumed that the mass spectrum is degenerate). However, in models with a single sterile state one instead has either $\delta N_{\text{eff},s}$ steriles with mass m_s and $3.046 + \delta N_{\text{eff}} - \delta N_{\text{eff},s}$ massless active states (NH) or $3.046 + \delta N_{\text{eff}} - \delta N_{\text{eff},s}$ massive active state with degenerate mass and $\delta N_{\text{eff},s}$ massless sterile states (IH). These two cases are different when it comes to structure formation and should in principle be treated separately (see e.g. [51] for a discussion about this point). Since the goal of this paper is to calculate δN_{eff} , not to provide quantitative constraints on specific models, we simply use δN_{eff} from this point on.

3.1 Numerical solution of the quantum kinetic equations

Solving the quantum kinetic equations numerically is non-trivial task. The number of differential equations are roughly $8N$ where N is the number of momentum bins, and since the resonances can be very narrow we need a few hundred points to obtain good precision. There are many vastly separated time-scales involved, so the problem is stiff, and once L changes, the system becomes extremely non-linear. We used two different solvers, one based on the numerical differentiation formulae of order 1–5 (`ndf15`) due to Shampine [52], and one based on the fifth order implicit Runge-Kutta method `RADAU5` due to Hairer and Wanner [53]. If the maximum order of the first method is reduced to two, both solvers are L-stable, and thus excellent for stiff problems. Because of the large number of equations and the sparsity of the Jacobian we must use sparse matrix methods for the linear algebra operations needed in both solvers. For this purpose, we are employing a small sparse matrix package based on [54].

To sample the momentum-space in an optimal way we are mapping the x -interval $[x_{\min}; x_{\max}]$ to a u -interval $[0; 1]$ by

$$u(x) = \frac{x - x_{\min}}{x_{\max} - x_{\min}} \times \frac{x_{\max} + x_{\text{ext}}}{x + x_{\text{ext}}}, \quad (3.3)$$

where x_{ext} is the extremal point of some moment of the Fermi-Dirac distribution. We chose the values $x_{\min} = 10^{-4}$, $x_{\text{ext}} = 3.1$ and $x_{\max} = 100$, and then sampled u uniformly. This is the same mapping employed in [55], but they go one step further and introduce an adaptive

grid that follows the resonances. This is not necessary for this project since our mixing angles are comparably larger, and we are not looking at chaotic amplification of an initially small value of L .

We evolved the system from an initial temperature of 60 MeV to a final temperature of 1 MeV for the following grid of masses and mixing angles:

$$10^{-3} \text{ eV}^2 \leq \delta m_s^2 \leq 10 \text{ eV}^2 \text{ and } 10^{-4} \leq \sin^2 2\theta_s \leq 10^{-1} \text{ for } L^{(a)} = 0, \quad (3.4a)$$

$$10^{-1} \text{ eV}^2 \leq \delta m_s^2 \leq 10 \text{ eV}^2 \text{ and } 10^{-3.3} \leq \sin^2 2\theta_s \leq 10^{-1} \text{ for } L^{(a)} = 10^{-2}. \quad (3.4b)$$

We ran the complete grids for different number of momentum bins, different accuracy parameters and both differential equation solvers with no noticeable difference.

3.2 Sterile neutrino production for zero lepton asymmetry

The simplest case, and the one most often studied in the literature, is the one where the lepton asymmetry is zero. For $L^{(a)} = 0$, the evolution of P_i^+ is decoupled from P_i^- [see Eqs. (2.20,2.23)] and the asymmetry remains zero for the whole evolution (as can be seen from Eq. (2.25)).

From Eqs. (A.4,A.8) in Appendix A it can be seen that there is either no resonance (NH) or that the resonances are identical for neutrinos and anti-neutrinos (IH). As it is well known, in IH the resonance propagates to higher values of x as the universe expands and eventually covers the entire momentum distribution of neutrinos.

In Fig. 1 we show the fraction of thermalised neutrinos, δN_{eff} , for the range of mixing parameters given in Eq. (3.4a) with initial asymmetry $L^{(\mu)} = 0$. The top panel shows the normal hierarchy, $\delta m_s^2 > 0$, and the bottom panel the inverted hierarchy, $\delta m_s^2 < 0$. The smaller parameter space described by (3.4b) is denoted with a dashed rectangle to facilitate comparison with the results presented in Sec 3.3.

We mark with a green hexagon the best fit point of the 3 + 1 global analysis presented in [56], obtained from a joint analysis of Solar, reactor, and short-baseline neutrino oscillation data $(\delta m_s^2, \sin^2 2\theta_s) = (0.9 \text{ eV}^2, 0.089)$. For that point $\delta N_{\text{eff}} = 1$ in both hierarchies, i.e. complete thermalization occurs. In addition we show the parameter range preferred by CMB and large scale structure (LSS) data. The 1–2–3 σ contours have been obtained interpolating the likelihood function obtained in [27] for each fixed δm_s^2 and N_{eff} . In both cases the lower left corners of parameter space where little thermalization occurs are disfavoured because of the CMB+LSS preference for extra energy density.

It is also of interest to see how the thermalization proceeds as a function of temperature. In Fig. 2 we show the evolution of δN_{eff} as a function of temperature for the NH scenario for a variety of different δm_s^2 and $\sin^2 2\theta_s$. For the non-resonant NH, the thermalization rate of sterile neutrinos is approximately $\Gamma_s \sim \frac{1}{2} \sin^2 2\theta_s \Gamma$. The maximum thermalisation rate occurs at a temperature of approximately $T_{\text{max}} \sim 10 (\delta m_s^2)^{1/6} \text{ MeV}$ and the final δN_{eff} depends only on $\sin^2 2\theta_m$ at that temperature (see [41] for a detailed discussion). In the top panel of Fig. 2 this behaviour can be seen. For very large vacuum mixing $\Gamma_s/H > 1$ already before T_{max} such that complete thermalisation has occurred already before T_{max} reached. For smaller mixing Γ_s/H never exceeds 1 and even though thermalisation proceeds fastest around T_{max} it is never fast enough to equilibrate the sterile states.

In the bottom panel the change in T_{max} as δm_s^2 varies is evident, and provided that T_{max} is higher than the active neutrino decoupling temperature the vacuum mixing in this case is large enough that complete thermalisation always occurs. For the non-resonant case

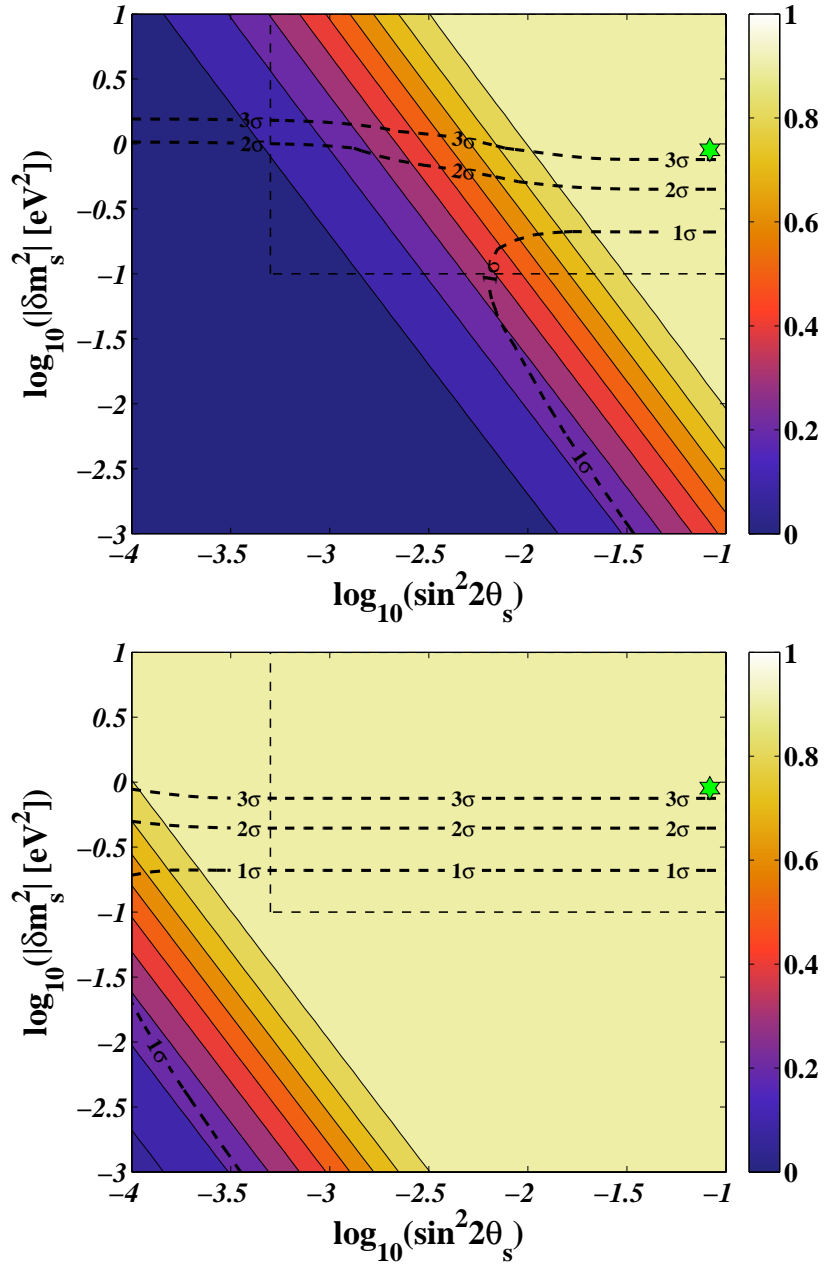


Figure 1. Iso- δN_{eff} contours in the $\sin^2 2\theta_s - \delta m_s^2$ plane for $L^{(\mu)} = 0$ and $\delta m_s^2 > 0$ (top panel) and $\delta m_s^2 < 0$ (bottom panel). The green hexagon denotes the ν_s best-fit mixing parameters as in the 3+1 global fit in [56]: $(\delta m_s^2, \sin^2 2\theta_s) = (0.9 \text{ eV}^2, 0.089)$. The 1 – 2 – 3 σ contours denote the CMB+LSS allowed regions for ν_s with sub-eV mass as in [27]. In order to facilitate the comparison with the results presented in Sec 3.3, a dashed rectangle denotes the parameter-space described by (3.4b).

the end result is that isocontours of δN_{eff} always lie at constant values of $\delta m_s^2 \sin^4 2\theta_s$, as can be seen in the top panel of Fig. 1.

In the inverted hierarchy the resonance conditions are always satisfied. Therefore, we expect full thermalization for a larger region of the mass-mixing parameters than in NH, as confirmed in Fig. 1. In this case, thermalisation may proceed through resonant conversions

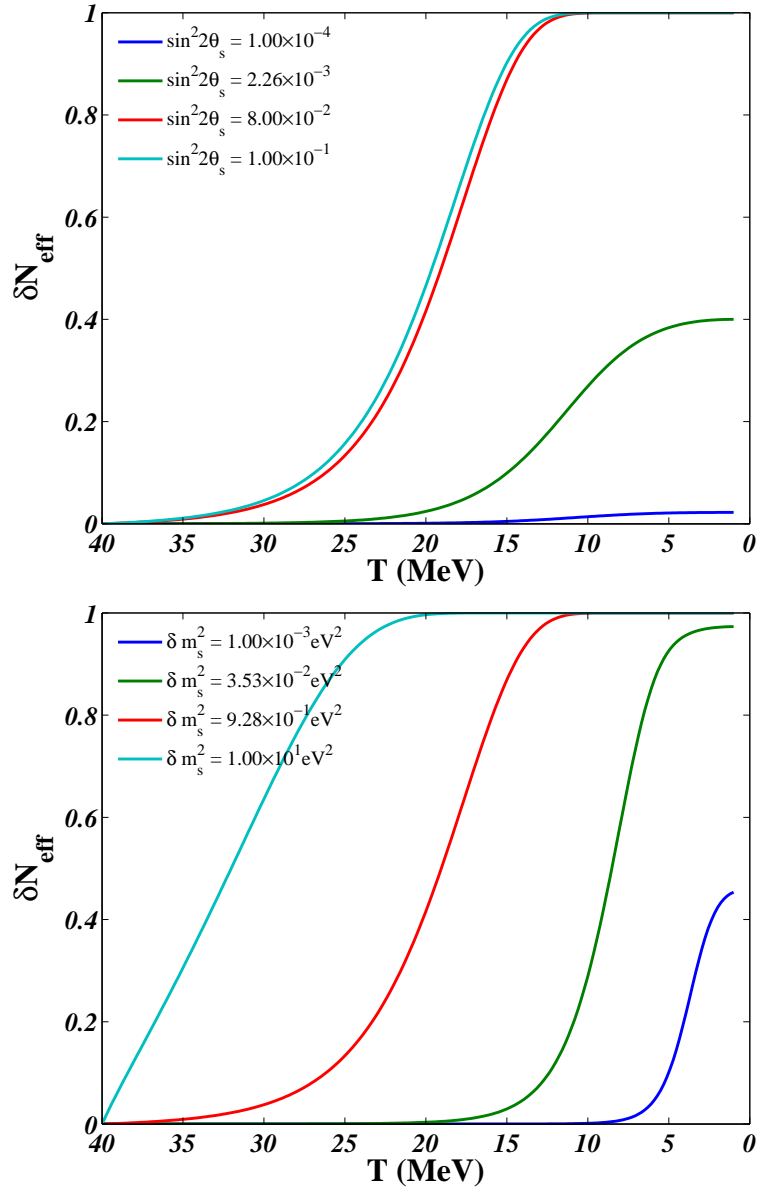


Figure 2. Top panel: δN_{eff} as a function of the temperature for four different mixing angles ($\sin^2 2\theta_s = 10^{-4}, 2 \times 10^{-3}, 5 \times 10^{-2}, 10^{-1}$) and fixed mass difference ($\delta m_s^2 = 0.93 \text{ eV}^2$). Bottom panel: δN_{eff} as a function of the temperature for four different mass differences ($\delta m_s^2 = 10^{-3}, 3.5 \times 10^{-2}, 9.3 \times 10^{-1}, 10 \text{ eV}^2$) and fixed mixing angle ($\sin^2 2\theta_s = 0.051$). Thermalisation begins earlier and is more effective for larger mass differences and for larger mixing angles.

alone. For illustration, we choose the point of Fig. 1 with $(\delta m_s^2, \sin^2 \theta_s) = (-3.3 \text{ eV}^2, 6 \times 10^{-4})$ for which $\delta N_{\text{eff}} = 0.55$ and we show the percentage of active (N_a) and sterile (N_s) neutrinos as a function of x for different T in Fig. 3. The thermalisation is not complete and it is nearly instantaneous as the resonance moves through the momentum spectrum and the resulting dip in the active sector is quickly repopulated from the background.

We have presented results for $L^{(\mu)} = 0$ only, but the case of $L^{(e)} = 0$ shows exactly the same trend as in Fig. 1. However, the region with $\delta N_{\text{eff}} = 1$ is slightly smaller than the one

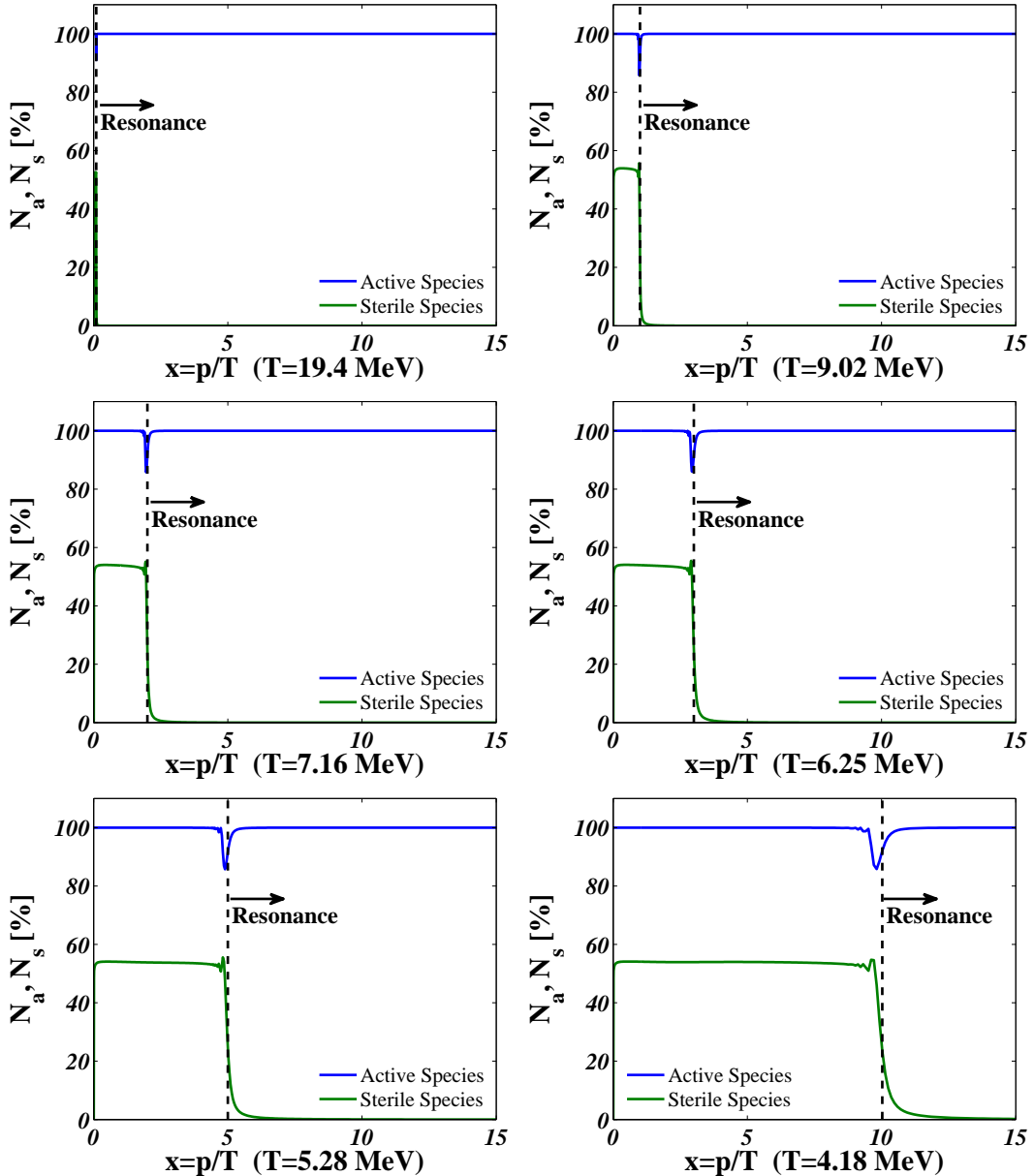


Figure 3. Temperature evolution of active and sterile neutrino distributions for the resonant case $(\delta m_s^2, \sin^2 \theta_s) = (-3.3 \text{ eV}^2, 6 \times 10^{-4})$ and $L^{(\mu)} = 0$.

shown in Fig. 1. This is due to the fact that ν_e 's have a larger potential than $\nu_{\mu,\tau}$ (because of the charged current interaction contribution) and therefore resonances occur at slight lower temperatures.

3.3 The case of large initial lepton asymmetry

We now discuss the thermalisation degree for initial large lepton asymmetry. In principle, one would expect a lepton asymmetry of the same order of magnitude as the baryon asymmetry ($\eta \simeq 10^{-10}$). However, since neutrinos are neutral particles, $L^{(a)} = 10^{-2} - 10^{-1}$ is not presently excluded [36, 37, 57] by the requirement of charge neutrality. A large lepton

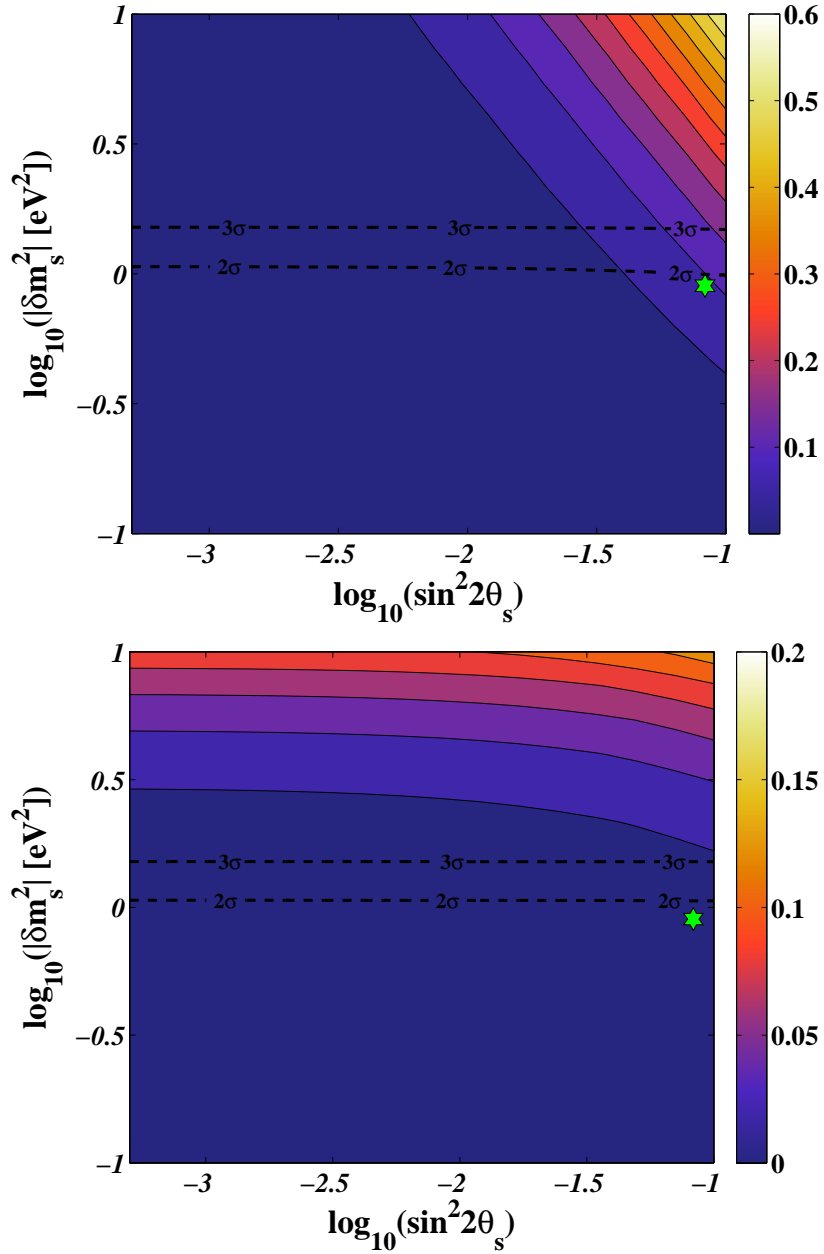


Figure 4. Iso- δN_{eff} contours in the $\sin^2 2\theta_s - \delta m_s^2$ plane for $L^{(\mu)} = 10^{-2}$ and $\delta m_s^2 > 0$ (top panel) and $\delta m_s^2 < 0$ (bottom panel), as in Fig. 1.

asymmetry is responsible for blocking the active-sterile flavor conversions by an in-medium suppression of the mixing angle; therefore it has been invoked as a means of significantly reducing the sterile abundance [31]. A large lepton number can be generated by e.g. an Affleck-Dine mechanism [58] or other models that are able to produce large lepton asymmetries and small baryonic ones [59, 60]. Another interesting possibility is to grow the lepton asymmetry from some initial $L^{(a)} \sim \mathcal{O}(10^{-10})$ using active-sterile oscillations [45, 61, 62]. Solving the QKE's in IH and with an initially small but non-zero lepton number, our preliminary results point toward a final lepton number varying between 10^{-5} and 10^{-2} depending

on the mixing parameters. For illustrative purposes, we choose to adopt $L^{(a)} = 10^{-2}$.

Figure 4 shows the δN_{eff} contour plot for $L^{(\mu)} = 10^{-2}$ and $\delta m_s^2 > 0$ (top panel) and $\delta m_s^2 < 0$ (bottom panel). The region with full thermalisation is now much smaller than in Fig. 1.

As we discuss in detail in Appendix A, a large value of $L^{(a)}$ confines the resonances to very small or large values of x , far away from the maximum of the active neutrino momentum distribution (see also [63]). Only at relatively low temperature does the resonance begin to move through the momentum distribution. What happens next is qualitatively very different for normal and inverted hierarchy. For NH the lepton asymmetry decreases as the resonance moves. This causes a run-away effect because as $L^{(a)}$ decreases the resonance moves faster, causing a faster decrease in $L^{(a)}$. When $L^{(a)}$ becomes less than approximately 10^{-5} (see Eq. (A.9)), the resonance disappears and the remaining evolution after this point is equivalent to the $L^{(a)} = 0$ NH case. For sufficiently large δm_s^2 and $\sin^2 2\theta_s$ the non-resonant production after the resonance disappears can be significant. However, the required mass difference and mixing to obtain the same degree of thermalisation are much larger than in the $L^{(a)} = 0$ case.

The rapid depletion of $L^{(a)}$ in NH causes the numerical solution to continue after this point with a very small time step. No further resonant production will occur after this point, but as we discuss above, some non-resonant thermalisation has yet to happen at this stage. To circumvent this problem, we stop the code when $L^{(a)}$ becomes very close to zero and restart it again with $L^{(a)} = 0$ using the static approximation discussed in Appendix B.

For IH the lepton asymmetry increases when the resonance moves, causing it to move slower and effectively blocking population of the sterile state until very late. For the range of mixing parameters studied here production of sterile neutrinos is effectively blocked until after the active species decouples, leading to a very small δN_{eff} . In Appendix A we give equations for the position of the resonances for finite $L^{(a)}$ along with useful approximations valid in different limits.

For ν_s mixing parameters as in [56], $\delta N_{\text{eff}} \sim 0$ in IH and $\delta N_{\text{eff}} = 0.05$ in NH. Constraints from BBN, CMB, and LSS have usually assumed a fully thermalised sterile state, but as also mentioned in [27] a finite lepton asymmetry can effectively block thermalisation and make this assumption invalid. In that case an eV sterile neutrino will not be in conflict with the cosmological neutrino mass bound, but of course the extra energy density preferred by CMB and LSS will then not be associable with the light sterile neutrino.

We finally note that since we have solved the quantum kinetic equations using the 1 sterile + 1 active approximation, only one lepton asymmetry is relevant in our equations (either e or μ). However, in the real 3+1 scenario there will be 3 separate flavour asymmetries and active-active oscillations will lead to some degree of equilibration between these asymmetries. While there will be some quantitative differences between our 1+1 treatment and the full 3+1 scenario we do expect the same qualitative behaviour, i.e. a blocking of thermalisation due to confinement of the active-sterile resonances.

4 Conclusions

Recent cosmological data seem to favor an excess of radiation beyond three neutrino families and photons, and light sterile neutrinos are possible candidates. The upcoming measurement of δN_{eff} by Planck will confirm or rule out the existence of such extra radiation with high precision [64, 65].

Light sterile neutrinos could thermalise prior to neutrino decoupling, contributing to the relativistic energy density in the early universe. Present data coming from CMB+LSS, and BBN allow the existence of one sub-eV mass sterile family but do not prefer extra fully thermalised sterile neutrinos in the eV-mass range since they violate the hot dark matter limit on the neutrino mass. However, the assumption of full thermalisation is not necessarily justified. In this paper, we have studied the evolution of active and sterile neutrinos in the early universe in order to calculate the effective number of thermalized species after $T \sim 1$ MeV when active neutrinos have decoupled and slightly before BBN commences. We have studied the amount of thermalisation for initial null and large ($L^{(a)} = 10^{-2}$) lepton asymmetry, for a range of mass-mixing parameters and for both normal and inverted mass hierarchies.

Assuming null initial lepton asymmetry, we find that the assumption of full thermalisation is justified for eV-mass sterile neutrinos with relatively large mixing (as suggested by short-baseline oscillation data). This inevitably leads to tension between CMB+LSS data which prefers very light sterile neutrinos and Solar, reactor and short-baseline data which prefers a mass around 1 eV or higher.

On the other hand, for large initial lepton asymmetries light sterile neutrinos are not (or only partially) thermalised for almost all the scanned parameter space. This provides a loophole for eV sterile neutrinos to be compatible with CMB+LSS constraints. For lepton asymmetries around 10^{-2} almost no thermalisation occurs for the parameters preferred by Solar, reactor and short-baseline data, and the sterile neutrinos would contribute very little to the current dark matter density.

One remaining open question neglected in this work is related to the impact of sterile neutrinos on BBN. The ν_e and $\bar{\nu}_e$ flux distributions are affected by active-sterile conversions and they enter the weak rates regulating the neutron-proton equilibrium (see [66] for a review on the topic). Therefore the ${}^4\text{He}$ abundance is sensitive to the presence of sterile families. In particular $\delta N_{\text{eff}} > 0$ and a less populated ν_e spectrum are both responsible for increasing the freeze-out temperature of the ratio n/p and therefore for a larger ${}^4\text{He}$ abundance.

For small $L^{(a)}$ and the mixing parameters discussed here the active-sterile oscillations occur well before BBN commences, while for large $L^{(a)}$ the active-sterile oscillations are no longer decoupled from the active ones and can occur close to the BBN temperature. We refer the reader to [67] for a discussion of BBN constraints on the sterile sector, but also stress that for large values of $L^{(a)}$ any quantitative exclusion limits in mixing parameter space would require solving the full QKEs including all three active species. This is clearly beyond the scope of the present paper, but remains an interesting and important calculation.

Note added: After the initial version of this paper was finalised, a semi-analytic estimate of the BBN effect in the 3+1 scenario using the quantum rate equations has appeared [68].

Acknowledgments

The authors are grateful to Georg G. Raffelt for valuable discussions. This work was partly supported by the Deutsche Forschungsgemeinschaft under the grant EXC-153 and by the European Union FP7 ITN INVISIBLES (Marie Curie Actions, PITN-GA-2011-289442). I.T. thanks the Alexander von Humboldt Foundation for support.

A Location of the resonances

Imposing the resonance condition for neutrinos ($V_z = 0$) and for antineutrinos ($\bar{V}_z = 0$), one finds the locations of the resonances [55]. In order to make explicit the x -dependence, we define

$$V_0 = \frac{\widetilde{V}_0}{x} \text{ and } V_1 = \widetilde{V}_1 x . \quad (\text{A.1})$$

Introducing

$$\ell = \begin{cases} \text{sign}[L^{(a)}] & \text{for particles} \\ -\text{sign}[L^{(a)}] & \text{for anti-particles} \end{cases} \quad (\text{A.2})$$

the resonance conditions ($V_z = 0$ and $\bar{V}_z = 0$) can be written

$$\widetilde{V}_1 x^2 + \ell |V_L| x + \widetilde{V}_0 = 0 . \quad (\text{A.3})$$

We define $m \equiv \text{sign}[\delta m_s^2]$ and write the solution in the following way

$$x_{\text{res}} = x_0 \left[A\ell \pm \sqrt{A^2 - m} \right] \equiv x_0 F_{\ell m}^{\pm}(A) , \quad (\text{A.4})$$

where we have defined

$$x_0 = \sqrt{\frac{m\widetilde{V}_0}{\widetilde{V}_1}} , \quad (\text{A.5})$$

$$A = \frac{|V_L|}{2\sqrt{m\widetilde{V}_0\widetilde{V}_1}} , \quad (\text{A.6})$$

$$F_{\ell m}^{\pm}(A) = \left[A\ell \pm \sqrt{A^2 - m} \right] . \quad (\text{A.7})$$

Note that x_0 is always real and positive. In order to have a physical solution, $F_{\ell m}^{\pm}$ has to be real and positive. This condition is satisfied for $F_{\pm 1, -1}^+(A)$ for any A and $F_{+1, +1}^{\pm}(A)$ for $A \geq 1$. Thus, we always have two physical solutions when $m = -1$, one for particles and one for anti-particles. On the other hand, when $m = +1$ and $A \geq 1$, we have two resonances: when $\ell > 0$, they occur for particles and when $\ell < 0$, they occur for anti-particles being in both cases responsible for destroying the lepton number. These equations reproduce the ones reported in [55] when $m = -1$.

We can expand the solutions for small and large $L^{(a)}$:

$$F_{-1, -1}^+ = -A + \sqrt{1 + A^2} \simeq \begin{cases} 1 - A + \frac{A^2}{2} - \dots & A \rightarrow 0^+ \\ \frac{1}{2A} - \dots & A \rightarrow \infty \end{cases} \quad (\text{A.8a})$$

$$F_{+1, -1}^+ = A + \sqrt{1 + A^2} \simeq \begin{cases} 1 + A + \frac{A^2}{2} - \dots & A \rightarrow 0^+ \\ 2A + \frac{1}{2A} - \dots & A \rightarrow \infty \end{cases} \quad (\text{A.8b})$$

$$F_{+1, +1}^+ = A + \sqrt{A^2 - 1} \simeq \begin{cases} 1 + \sqrt{2}\sqrt{A-1} + \dots & A \rightarrow 1^+ \\ 2A - \frac{1}{2A} - \dots & A \rightarrow \infty \end{cases} \quad (\text{A.8c})$$

$$F_{+1, +1}^- = A - \sqrt{A^2 - 1} \simeq \begin{cases} 1 - \sqrt{2}\sqrt{A-1} + \dots & A \rightarrow 1^+ \\ \frac{1}{2A} - \dots & A \rightarrow \infty \end{cases} \quad (\text{A.8d})$$

with A and x_0 assuming the following expressions

$$\begin{aligned}
A &= \frac{6\zeta(3)}{\pi^3} \sqrt{\frac{10}{7\sqrt{2}}} \frac{T |L^{(a)}| M_z \sqrt{G_F}}{\sqrt{\cos 2\theta_s |\delta m_s^2| (n_\nu + n_{\bar{\nu}}) g}} \\
&\simeq 7.28 \times 10^4 T_{\text{MeV}} \frac{|L^{(a)}|}{\sqrt{\cos 2\theta_s |\delta m_s^2|_{\text{eV}^2} (n_\nu + n_{\bar{\nu}}) g}} \\
x_0 &= \frac{3}{\pi} \sqrt{\frac{5}{7\sqrt{2}}} \frac{M_z}{\sqrt{G_F} T^3} \sqrt{\frac{\cos 2\theta_s |\delta m_s^2|}{(n_\nu + n_{\bar{\nu}}) g}} \simeq 1.81 \times 10^4 T_{\text{MeV}}^{-3} \sqrt{\frac{\cos 2\theta_s |\delta m_s^2|_{\text{eV}^2}}{(n_\nu + n_{\bar{\nu}}) g}}.
\end{aligned} \tag{A.9}$$

For $L^{(a)} = 10^{-2}$ we have $A \gg 1$ and therefore the lowest resonance will be

$$x_{\text{res,low}} \simeq \frac{x_0}{2A} = \frac{\pi^2 \cos 2\theta_s |\delta m_s^2|}{4\sqrt{2}\zeta(3) T^4 |L^{(a)}| G_F} \simeq 0.12 \frac{\cos 2\theta_s |\delta m_s^2|_{\text{eV}^2}}{T_{\text{MeV}}^4 |L^{(a)}|}. \tag{A.10}$$

Note that $x_{\text{res,low}}$ is independent on the sign of the mass hierarchy and the total neutrino density. Moreover, from the previous equation, we can extract the temperature at which the lowest resonance starts sweeping the bulk of the Fermi-Dirac distribution. This provides a good estimate of when resonant thermalisation sets in. For example, in the limit of large lepton number, assuming $x_{\text{res,low}} \simeq 0.1$, we find $T_{\text{res,low}} \simeq 3$ MeV for $(\delta m_s^2, \sin^2 2\theta_s) = (1 \text{ eV}^2, 10^{-2})$. On the other hand, the higher resonance has no effect at all. In fact

$$x_{\text{res,high}} \simeq x_0 \times 2A = \frac{180\zeta(3) |L^{(a)}| M_z^2}{7\pi^2 T_{\text{MeV}}^2 (n_\nu + n_{\bar{\nu}}) g} \simeq 2.6 \times 10^{10} \frac{|L^{(a)}|}{(n_\nu + n_{\bar{\nu}}) g T_{\text{MeV}}^2}. \tag{A.11}$$

Therefore, for $L^{(a)} = 0.01$, $x_{\text{res,high}}$ will pass through the peak of the Fermi-Dirac distribution at $T \simeq 1$ GeV. At that temperature, the damping term is so strong that no oscillations occur and thermalisation is inhibited.

B Adiabatic approximation

The so-called ‘‘adiabatic’’ approximation was first introduced in [69] and, under certain conditions, it allows one to derive an approximate analytic solution of the QKE’s. In this section, we closely follow the derivation from first principles of [49]. Such derivation assumes that the rate of repopulation (\dot{P}_0) vanishes, however the more careful analysis of [70], including a non-zero repopulation rate, turns out to give the same final formula for P_y . Therefore we choose to adopt the simpler derivation.

Assuming $\dot{P}_0 = 0$, Eq. (2.4) can be written as a homogeneous matrix equation:

$$\frac{d}{dt} \begin{bmatrix} P_x \\ P_y \\ P_z \end{bmatrix} = \begin{bmatrix} -D & -V_z & 0 \\ V_z & -D & -V_x \\ 0 & V_x & 0 \end{bmatrix} P_z, \tag{B.1}$$

or using a vectorial notation

$$\frac{d\mathbf{P}}{dt} = \mathcal{K}\mathbf{P}. \tag{B.2}$$

The matrix \mathcal{K} can be diagonalised by a time-dependent matrix \mathcal{U} , such that $\mathcal{U}\mathcal{K}\mathcal{U}^{-1} = \mathcal{D}$. The matrix \mathcal{U} defines an instantaneous diagonal basis through $\mathbf{Q} \equiv \mathcal{U}\mathbf{P}$ and, in principle, the evolution equation for \mathbf{Q} is non-trivial:

$$\frac{d\mathbf{Q}}{dt} = \mathcal{K}\mathbf{Q} - \mathcal{U} \frac{d\mathcal{U}^{-1}}{dt} \mathbf{Q}. \tag{B.3}$$

However, if we assume that Eq. (B.3) is dominated by the first term, the differential equation can be easily solved. This is the so-called ‘‘adiabatic’’ approximation and its applicability has been analysed thoroughly in [49]. Quoting [49], it is applicable when

$$\frac{V_x}{\sqrt{D^2 + V_z^2}} \ll 1, \quad (\text{B.4a})$$

$$T \ll 3\text{MeV}, \quad (\text{B.4b})$$

$$\left| \frac{dL^{(a)}}{dT_{\text{MeV}}} \right| \ll 5 \times 10^{-11} T_{\text{MeV}}^4. \quad (\text{B.4c})$$

Equation (B.4a) is not easily stated as just a limit on temperature. If we are not close to the resonance and V_z is dominated by V_0 , we find $\tan 2\theta_s \ll 1$ which is true for our parameter space. If we are close to the resonance, the criterion depends on $L^{(a)}$ through x_{res} (see Appendix A for a discussion of the position of the resonances). Using Eqs. (A.4,A.8), we find

$$L^{(a)} \gg 10^{-5} : \frac{|V_x|}{D} \gtrsim \frac{|\delta m_s^2| \sin 2\theta_s}{C_a G_F^2 x_{\text{res,low}}^2 T^6} \sim 5 \times 10^{11} \frac{T_{\text{MeV}}^2 \sin 2\theta_s}{|\delta m_s^2| \cos^2 2\theta_s} L^{(a)2}, \quad (\text{B.5})$$

$$L^{(a)} \ll 10^{-5} : \frac{|V_x|}{D} \gtrsim \frac{|\delta m_s^2| \sin 2\theta_s}{C_a G_F^2 x_0^2 T^6} \sim 50 \tan 2\theta_s. \quad (\text{B.6})$$

For large $L^{(a)}$, we almost always break the approximation at the lowest resonance. But, since the resonance occurs at a very low momentum, it would have no effect on the physics anyway. In principle, it could still affect numerics but we did not encounter problems on this particular front. For small $L^{(a)}$, we are safe for most of the parameter space and, as for large $L^{(a)}$, if the resonance is not sitting in a populated part of the Fermi-Dirac distribution, there should not be any impact on the physics from breaking this approximation slightly. This also applies to the third condition: If the resonance is not in the middle of a populated part of the distribution, we do not have a fast evolution of $L^{(a)}$ and the approximation is valid.

Equation (B.3) can be formally solved by

$$Q_i(t) = \exp\left(\int_{t_0}^t k_i(t') dt'\right) Q_i(t_0), \quad (\text{B.7})$$

where the k_i 's are the eigenvalues of \mathcal{K} . Expanding those to lowest order in V_x , we have

$$k_1 = -D + iV_z, \quad k_2 = -D - iV_z, \quad k_3 = -\frac{V_x^2 D}{D^2 + V_z^2}. \quad (\text{B.8})$$

Assuming that D is large and V_x satisfies Eq. (B.4a), we find

$$Q_1(t) = Q_2(t) = 0, \quad Q_3(t) = Q_3(t_0). \quad (\text{B.9})$$

The adiabatic approximation allows us to relate P_x , P_y and P_z through

$$\begin{bmatrix} P_x(t) \\ P_y(t) \\ P_z(t) \end{bmatrix} = \mathcal{U}^{-1}(t) \begin{bmatrix} Q_1(t) \\ Q_2(t) \\ Q_3(t) \end{bmatrix} = \mathcal{U}^{-1}(t) \begin{bmatrix} 0 \\ 0 \\ Q_3(t_0) \end{bmatrix} = Q_3(t_0) \mathbf{s}_3(t), \quad (\text{B.10})$$

where $\mathbf{s}_3(t)$ is the third column in $\mathcal{U}^{-1}(t)$ which is also the normalised eigenvector corresponding to k_3 . We have

$$\mathbf{s}_3(t) = N \begin{bmatrix} 1 \\ -(D + k_3)/V_z \\ -V_x(D + k_3)/(V_z k_3) \end{bmatrix}, \quad (\text{B.11})$$

with N a normalisation constant. We can now relate P_x and P_y to P_z to lowest order in V_x :

$$P_x(t) = \frac{V_x V_z}{D^2 + V_z^2} P_z(t), \quad (\text{B.12})$$

$$P_y(t) = -\frac{V_x D}{D^2 + V_z^2} P_z(t). \quad (\text{B.13})$$

Substituting V_z by \bar{V}_z gives the corresponding relations for anti-particles.

References

- [1] **LSND** Collaboration, A. Aguilar-Arevalo *et al.*, “Evidence for neutrino oscillations from the observation of anti- ν /e appearance in a anti- ν / μ beam,” *Phys. Rev.* **D64** (2001) 112007, [arXiv:hep-ex/0104049](#).
- [2] A. Strumia, “Interpreting the LSND anomaly: sterile neutrinos or CPT- violation or...?,” *Phys. Lett.* **B539** (2002) 91–101, [arXiv:hep-ph/0201134](#).
- [3] M. C. Gonzalez-Garcia and M. Maltoni, “Phenomenology with Massive Neutrinos,” *Phys. Rept.* **460** (2008) 1–129, [arXiv:0704.1800](#) [[hep-ph](#)].
- [4] **MiniBooNE** Collaboration, A. A. Aguilar-Arevalo *et al.*, “Unexplained Excess of Electron-Like Events From a 1-GeV Neutrino Beam,” *Phys. Rev. Lett.* **102** (2009) 101802, [arXiv:0812.2243](#) [[hep-ex](#)].
- [5] **MiniBooNE** Collaboration, A. A. Aguilar-Arevalo *et al.*, “A Search for Electron Antineutrino Appearance at the $\Delta m^2 \sim 1 \text{ eV}^2$ Scale,” *Phys. Rev. Lett.* **103** (2009) 111801, [arXiv:0904.1958](#) [[hep-ex](#)].
- [6] G. Karagiorgi, Z. Djurcic, J. M. Conrad, M. H. Shaevitz, and M. Sorel, “Viability of $\Delta m^2 \sim 1 \text{ eV}^2$ sterile neutrino mixing models in light of MiniBooNE electron neutrino and antineutrino data from the Booster and NuMI beamlines,” *Phys. Rev.* **D80** (2009) 073001, [arXiv:0906.1997](#) [[hep-ph](#)].
- [7] E. Akhmedov and T. Schwetz, “MiniBooNE and LSND data: non-standard neutrino interactions in a (3+1) scheme versus (3+2) oscillations,” *JHEP* **10** (2010) 115, [arXiv:1007.4171](#) [[hep-ph](#)].
- [8] G. Mention *et al.*, “The Reactor Antineutrino Anomaly,” *Phys. Rev.* **D83** (2011) 073006, [arXiv:1101.2755](#) [[hep-ex](#)].
- [9] P. Huber, “On the determination of anti-neutrino spectra from nuclear reactors,” *Phys. Rev.* **C84** (2011) 024617, [arXiv:1106.0687](#) [[hep-ph](#)].
- [10] J. Kopp, M. Maltoni, and T. Schwetz, “Are there sterile neutrinos at the eV scale?,” *Phys. Rev. Lett.* **107** (2011) 091801, [arXiv:1103.4570](#) [[hep-ph](#)].
- [11] S. Razzaque and A. Y. Smirnov, “Searching for sterile neutrinos in ice,” *JHEP* **07** (2011) 084, [arXiv:1104.1390](#) [[hep-ph](#)].
- [12] J. Hamann, S. Hannestad, G. G. Raffelt, and Y. Y. Y. Wong, “Observational bounds on the cosmic radiation density,” *JCAP* **0708** (2007) 021, [arXiv:0705.0440](#) [[astro-ph](#)].

- [13] J. Hamann, S. Hannestad, J. Lesgourgues, C. Rampf, and Y. Y. Y. Wong, “Cosmological parameters from large scale structure - geometric versus shape information,” *JCAP* **1007** (2010) 022, [arXiv:1003.3999 \[astro-ph.CO\]](#).
- [14] M. C. Gonzalez-Garcia, M. Maltoni, and J. Salvado, “Robust Cosmological Bounds on Neutrinos and their Combination with Oscillation Results,” *JHEP* **08** (2010) 117, [arXiv:1006.3795 \[hep-ph\]](#).
- [15] G. Mangano *et al.*, “Relic neutrino decoupling including flavour oscillations,” *Nucl. Phys.* **B729** (2005) 221–234, [arXiv:hep-ph/0506164](#).
- [16] WMAP Collaboration, E. Komatsu *et al.*, “Seven-Year Wilkinson Microwave Anisotropy Probe (WMAP) Observations: Cosmological Interpretation,” *Astrophys. J. Suppl.* **192** (2011) 18, [arXiv:1001.4538 \[astro-ph.CO\]](#).
- [17] J. Dunkley, R. Hlozek, J. Sievers, V. Acquaviva, P. Ade, *et al.*, “The Atacama Cosmology Telescope: Cosmological Parameters from the 2008 Power Spectra,” *Astrophys. J.* **739** (2011) 52, [arXiv:1009.0866 \[astro-ph.CO\]](#).
- [18] R. Keisler, C. Reichardt, K. Aird, B. Benson, L. Bleem, *et al.*, “A Measurement of the Damping Tail of the Cosmic Microwave Background Power Spectrum with the South Pole Telescope,” *Astrophys. J.* **743** (2011) 28, [arXiv:1105.3182 \[astro-ph.CO\]](#).
- [19] J. Hamann, “Evidence for extra radiation? Profile likelihood versus Bayesian posterior,” *JCAP* **1203** (2012) 021, [arXiv:1110.4271 \[astro-ph.CO\]](#).
- [20] S. Joudaki, “Constraints on Neutrino Mass and Light Degrees of Freedom in Extended Cosmological Parameter Spaces,” [arXiv:1202.0005 \[astro-ph.CO\]](#).
- [21] E. Giusarma, M. Archidiacono, R. de Putter, A. Melchiorri, and O. Mena, “Sterile neutrino models and nonminimal cosmologies,” *Phys. Rev.* **D85** (2012) 083522, [arXiv:1112.4661 \[astro-ph.CO\]](#).
- [22] K. M. Nollett and G. P. Holder, “An analysis of constraints on relativistic species from primordial nucleosynthesis and the cosmic microwave background,” [arXiv:1112.2683 \[astro-ph.CO\]](#).
- [23] A. X. Gonzalez-Morales, R. Poltis, B. D. Sherwin, and L. Verde, “Are priors responsible for cosmology favoring additional neutrino species?,” [arXiv:1106.5052 \[astro-ph.CO\]](#).
- [24] Y. I. Izotov and T. X. Thuan, “The primordial abundance of 4He : evidence for non-standard big bang nucleosynthesis,” *Astrophys. J.* **710** (2010) L67–L71, [arXiv:1001.4440 \[astro-ph.CO\]](#).
- [25] E. Aver, K. A. Olive, and E. D. Skillman, “A New Approach to Systematic Uncertainties and Self-Consistency in Helium Abundance Determinations,” *JCAP* **1005** (2010) 003, [arXiv:1001.5218 \[astro-ph.CO\]](#).
- [26] J. Hamann, S. Hannestad, G. G. Raffelt, and Y. Y. Y. Wong, “Sterile neutrinos with eV masses in cosmology – how disfavoured exactly?,” *JCAP* **1109** (2011) 034, [arXiv:1108.4136 \[astro-ph.CO\]](#).
- [27] J. Hamann, S. Hannestad, G. G. Raffelt, I. Tamborra, and Y. Y. Y. Wong, “Cosmology Favoring Extra Radiation and Sub-eV Mass Sterile Neutrinos as an Option,” *Phys. Rev. Lett.* **105** (2010) 181301, [arXiv:1006.5276 \[hep-ph\]](#).
- [28] E. Giusarma *et al.*, “Constraints on massive sterile neutrino species from current and future cosmological data,” *Phys. Rev.* **D83** (2011) 115023, [arXiv:1102.4774 \[astro-ph.CO\]](#).
- [29] Z. Hou, R. Keisler, L. Knox, M. Millea, and C. Reichardt, “How Additional Massless Neutrinos Affect the Cosmic Microwave Background Damping Tail,” [arXiv:1104.2333 \[astro-ph.CO\]](#).
- [30] S. Dodelson, A. Melchiorri, and A. Slosar, “Is cosmology compatible with sterile neutrinos?,”

- Phys.Rev.Lett.* **97** (2006) 041301, [arXiv:astro-ph/0511500](#) [[astro-ph](#)].
- [31] Y.-Z. Chu and M. Cirelli, “Sterile neutrinos, lepton asymmetries, primordial elements: How much of each?,” *Phys.Rev.* **D74** (2006) 085015, [arXiv:astro-ph/0608206](#) [[astro-ph](#)].
- [32] A. Melchiorri, O. Mena, S. Palomares-Ruiz, S. Pascoli, A. Slosar, *et al.*, “Sterile Neutrinos in Light of Recent Cosmological and Oscillation Data: A Multi-Flavor Scheme Approach,” *JCAP* **0901** (2009) 036, [arXiv:0810.5133](#) [[hep-ph](#)].
- [33] K. Abazajian, N. F. Bell, G. M. Fuller, and Y. Y. Y. Wong, “Cosmological lepton asymmetry, primordial nucleosynthesis, and sterile neutrinos,” *Phys. Rev.* **D72** (2005) 063004, [arXiv:astro-ph/0410175](#).
- [34] H.-S. Kang and G. Steigman, “Cosmological constraints on neutrino degeneracy,” *Nucl.Phys.* **B372** (1992) 494–520.
- [35] V. Simha and G. Steigman, “Constraining The Universal Lepton Asymmetry,” *JCAP* **0808** (2008) 011, [arXiv:0806.0179](#) [[hep-ph](#)].
- [36] E. Castorina, U. Franca, M. Lattanzi, J. Lesgourgues, G. Mangano, *et al.*, “Cosmological lepton asymmetry with a nonzero mixing angle θ_{13} ,” [arXiv:1204.2510](#) [[astro-ph.CO](#)].
- [37] A. Dolgov, S. Hansen, S. Pastor, S. Petcov, G. Raffelt, *et al.*, “Cosmological bounds on neutrino degeneracy improved by flavor oscillations,” *Nucl.Phys.* **B632** (2002) 363–382, [arXiv:hep-ph/0201287](#) [[hep-ph](#)].
- [38] Y. Y. Wong, “Analytical treatment of neutrino asymmetry equilibration from flavor oscillations in the early universe,” *Phys.Rev.* **D66** (2002) 025015, [arXiv:hep-ph/0203180](#) [[hep-ph](#)].
- [39] K. N. Abazajian, J. F. Beacom, and N. F. Bell, “Stringent constraints on cosmological neutrino anti-neutrino asymmetries from synchronized flavor transformation,” *Phys.Rev.* **D66** (2002) 013008, [arXiv:astro-ph/0203442](#) [[astro-ph](#)].
- [40] L. Stodolsky, “On the Treatment of Neutrino Oscillations in a Thermal Environment,” *Phys. Rev.* **D36** (1987) 2273.
- [41] K. Enqvist, K. Kainulainen, and M. J. Thomson, “Stringent cosmological bounds on inert neutrino mixing,” *Nucl.Phys.* **B373** (1992) 498–528.
- [42] B. H. J. McKellar and M. J. Thomson, “Oscillating doublet neutrinos in the early universe,” *Phys. Rev.* **D49** (1994) 2710–2728.
- [43] G. Sigl and G. G. Raffelt, “General kinetic description of relativistic mixed neutrinos,” *Nucl. Phys.* **B406** (1993) 423–451.
- [44] D. Boyanovsky and C. Ho, “Production of a sterile species: Quantum kinetics,” *Phys.Rev.* **D76** (2007) 085011, [arXiv:0705.0703](#) [[hep-ph](#)].
- [45] R. Barbieri and A. Dolgov, “Neutrino oscillations in the early universe,” *Nucl.Phys.* **B349** (1991) 743–753.
- [46] K. Enqvist, K. Kainulainen, and J. Maalampi, “Refraction and oscillations of neutrinos in the early universe,” *Nucl. Phys.* **B349** (1991) 754–790.
- [47] K. Enqvist, K. Kainulainen, and J. Maalampi, “Resonant neutrino transitions and nucleosynthesis,” *Phys. Lett.* **B249** (1990) 531–534.
- [48] D. Notzold and G. G. Raffelt, “Neutrino Dispersion at Finite Temperature and Density,” *Nucl. Phys.* **B307** (1988) 924.
- [49] N. F. Bell, R. R. Volkas, and Y. Y. Y. Wong, “Relic neutrino asymmetry evolution from first principles,” *Phys. Rev.* **D59** (1999) 113001, [arXiv:hep-ph/9809363](#).
- [50] P. Di Bari and R. Foot, “On the sign of the neutrino asymmetry induced by active- sterile neutrino oscillations in the early universe,” *Phys. Rev.* **D61** (2000) 105012,

[arXiv:hep-ph/9912215](#).

- [51] S. Hannestad and G. G. Raffelt, “Neutrino masses and cosmic radiation density: Combined analysis,” *JCAP* **0611** (2006) 016, [arXiv:astro-ph/0607101](#) [[astro-ph](#)].
- [52] L. F. Shampine and M. W. Reichelt, “The MATLAB ODE Suite,” *SIAM J. Sci. Comput.* **18** (1997) no. 1, 1–22.
<http://dx.doi.org/10.1137/S1064827594276424>.
- [53] E. Hairer, S. Nørsett, and G. Wanner, *Solving Ordinary Differential Equations: Stiff and differential-algebraic problems*. Springer series in computational mathematics. Springer-Verlag, 1993.
- [54] T. A. Davis, *Direct Methods for Sparse Linear Systems (Fundamentals of Algorithms 2)*. Society for Industrial and Applied Mathematics, Philadelphia, PA, USA, 2006.
- [55] K. Kainulainen and A. Sorri, “Oscillation induced neutrino asymmetry growth in the early universe,” *JHEP* **02** (2002) 020, [arXiv:hep-ph/0112158](#).
- [56] C. Giunti and M. Laveder, “Implications of 3+1 Short-Baseline Neutrino Oscillations,” *Phys.Lett.* **B706** (2011) 200–207, [arXiv:1111.1069](#) [[hep-ph](#)].
- [57] S. Pastor, T. Pinto, and G. G. Raffelt, “Relic density of neutrinos with primordial asymmetries,” *Phys.Rev.Lett.* **102** (2009) 241302, [arXiv:0808.3137](#) [[astro-ph](#)].
- [58] M. Kawasaki, F. Takahashi, and M. Yamaguchi, “Large lepton asymmetry from Q balls,” *Phys.Rev.* **D66** (2002) 043516, [arXiv:hep-ph/0205101](#) [[hep-ph](#)].
- [59] J. A. Harvey and E. W. Kolb, “GRAND UNIFIED THEORIES AND THE LEPTON NUMBER OF THE UNIVERSE,” *Phys.Rev.* **D24** (1981) 2090.
- [60] A. Dolgov, “Neutrinos in cosmology,” *Phys.Rept.* **370** (2002) 333–535, [arXiv:hep-ph/0202122](#) [[hep-ph](#)].
- [61] R. Foot, M. J. Thomson, and R. Volkas, “Large neutrino asymmetries from neutrino oscillations,” *Phys.Rev.* **D53** (1996) 5349–5353, [arXiv:hep-ph/9509327](#) [[hep-ph](#)].
- [62] R. Barbieri and A. Dolgov, “Bounds on Sterile-neutrinos from Nucleosynthesis,” *Phys.Lett.* **B237** (1990) 440.
- [63] X.-D. Shi and G. M. Fuller, “A new dark matter candidate: Non-thermal sterile neutrinos,” *Phys. Rev. Lett.* **82** (1999) 2832–2835, [arXiv:astro-ph/9810076](#).
- [64] L. Perotto, J. Lesgourgues, S. Hannestad, H. Tu, and Y. Y. Wong, “Probing cosmological parameters with the CMB: Forecasts from full Monte Carlo simulations,” *JCAP* **0610** (2006) 013, [arXiv:astro-ph/0606227](#) [[astro-ph](#)].
- [65] J. Hamann, J. Lesgourgues, and G. Mangano, “Using BBN in cosmological parameter extraction from CMB: A Forecast for PLANCK,” *JCAP* **0803** (2008) 004, [arXiv:0712.2826](#) [[astro-ph](#)].
- [66] G. Steigman, “Primordial Nucleosynthesis in the Precision Cosmology Era,” *Ann.Rev.Nucl.Part.Sci.* **57** (2007) 463–491, [arXiv:0712.1100](#) [[astro-ph](#)].
- [67] A. Dolgov and F. Villante, “BBN bounds on active sterile neutrino mixing,” *Nucl.Phys.* **B679** (2004) 261–298, [arXiv:hep-ph/0308083](#) [[hep-ph](#)].
- [68] A. Mirizzi, N. Saviano, G. Miele, and P. D. Serpico, “Light sterile neutrino production in the early universe with dynamical neutrino asymmetries,” [arXiv:1206.1046](#) [[hep-ph](#)].
- [69] R. Foot and R. Volkas, “Studies of neutrino asymmetries generated by ordinary sterile neutrino oscillations in the early universe and implications for big bang nucleosynthesis bounds,” *Phys.Rev.* **D55** (1997) 5147–5176, [arXiv:hep-ph/9610229](#) [[hep-ph](#)].
- [70] K. S. Lee, R. R. Volkas, and Y. Y. Wong, “Further studies on relic neutrino asymmetry

generation. 2. A Rigorous treatment of repopulation in the adiabatic limit,”
Phys.Rev. **D62** (2000) 093025, [arXiv:hep-ph/0007186](#) [[hep-ph](#)].